LAWRENCE
LIVERMORE
NATIONAL
LABORATORY

LLNL-TR-417075

A tantalum strength model using a multiscale approach: version 2

R. Becker, A. Arsenlis, G. Hommes, J. Marian, M. Rhee, L. H. Yang

September 23, 2009

Disclaimer

This work performed under the auspices of the U.S. Department of Energy by Lawrence Livermore National Laboratory under Contract DE-AC52-07NA27344.

A tantalum strength model using a multiscale approach: version 2

R. Becker, A. Arsenlis, G. Hommes, J. Marian, M. Rhee, and L. Yang

Lawrence Livermore National Laboratory
7000 East Avenue, P.O. Box 808, Livermore, CA 94550

Introduction

A continuum strength model for tantalum was developed in 2007 using a multiscale approach[1]. This was our first attempt at connecting simulation results from atomistic to continuum length scales, and much was learned that we were not able to incorporate into the model at that time. The tantalum model described in this report represents a second cut at pulling together multiscale simulation results into a continuum model. Insight gained in creating previous multiscale models for tantalum and vanadium [2] was used to guide the model construction and functional relations for the present model. While the basic approach follows that of the vanadium model, there are significant departures. Some of the recommendations from the vanadium report were followed, but not all. Results from several new analysis techniques have not yet been incorporated due to technical difficulties.

Molecular dynamics simulations of single dislocation motion at several temperatures suggested that the thermal activation barrier was temperature dependent [2]. This dependency required additional temperature functions be included within the assumed Arrhenius relation. The combination of temperature dependent functions created a complex model with a non unique parameterization and extra model constants. The added complexity had no tangible benefits. The recommendation was to abandon the strict Arrhenius form and create a simpler curve fit to the molecular dynamics data for shear stress versus dislocation velocity [2].

Functions relating dislocation velocity and applied shear stress were constructed vor vanadium for both edge and screw dislocations [2]. However, an attempt to formulate a robust continuum constitutive model for vanadium using both dislocation populations was unsuccessful; the level of coupling achieved was inadequate to constrain the dislocation evolution properly. Since the behavior of BCC materials is typically assumed to be dominated by screw dislocations, the constitutive relations were ultimately built using only the screw relations. In light of this, the screw dislocation mobility relation is chosen as the starting point for the present tantalum model. Edge dislocations are not included explicitly in the current model.

A significant change from the previous models is in the functional dependence of the dislocation evolution equations. The prior multiscale models assumed that the dislocation evolution rate depended on stress as well dislocation velocity. This crated an implicit dependence on the kinetic relation and required an iterative solution for the dislocation density. In the present model the integration scheme is simplified by casting the dislocation evolution terms of strain rate and current dislocation density.

The final notable change was in the transition relation from the thermally activated regime to phonon drag. Historically, and in the prior models, this transition had been through a harmonic average on the strain rates making it impossible to determine the stress directly when given the plastic strain rate. After considering alternative transition relations, it was determined that an

equally suitable fit to the molecular dynamics simulation data in the transition region could be constructed by averaging stresses rather than strain rates.

The end result of these enhancements is a simpler (fewer parameters) and more straight forward model formulation where the material strength can be evaluated directly when given the plastic strain rate, temperature, pressure and the dislocation density at the beginning of the time step. This greatly improves the computational efficiency and robustness over the prior models where additional iteration loops were required.

Model Construction

The basis for the macroscale model is plastic deformation by thermally activated dislocation motion and strain hardening resulting from elastic interactions among dislocations. The connection between dislocation mechanics and macroscale plasticity variables is through traditional models. Dislocation density is evolved as the state variable that characterizes the flow strength of the material. The primary focus for the model is the temperature, strain rate and pressure dependence of the plastic flow strength. Microstructure and mechanisms at the grain scale are neglected, and the material is assumed to be isotropic following J2-Flow theory plasticity with an associative flow rule.

Connection to continuum variables

The average dislocation velocity, v, on a particular slip system is assumed to be related to the macroscopic plastic strain rate, $\dot{\varepsilon}^p$, through Orowan's relation,

$$v = \frac{\dot{\varepsilon}^p M}{\eta \rho b} \tag{1}$$

where M is the Taylor factor, ρ the dislocation density, b the Burger's vector, and η an order-one constant. Many descriptions of the Orowan relation emphasize that the mobile dislocation density should be utilized. However, within the context of the dislocation dynamics simulations that are used as the basis for the continuum model, there is no distinction between mobile and immobile dislocations; some dislocations just have a velocity near zero. Hence, the velocity in Eq. 1 represents some average of a velocity distribution.

The von Mises effective stress, σ_e, is assumed to be related to resolved shear stress on the slip systems through the Taylor factor.

$$\sigma_e = M\left[\left(\tau_a + \phi_A \hat{\tau}(\rho)\right) + \tau^* \left(\tau_p + \phi_T \hat{\tau}(\rho)\right)\right] \tag{2}$$

The strength is partitioned into athermal and thermal contributions given by the first and second terms in the square brackets, respectively. In the first term, $\tau_a$is the athermal stress representing some inherent crystal lattice resistance to dislocation motion. It does not depend on strain rate or temperature. The rate and temperature independent strengthening due to forest dislocations is included through $\hat{\tau}(\rho)$. In the thermal contribution, τ^* is a dimensionless multiplier accounting for temperature and strain rate dependence of dislocation glide. It multiplies a base strength that is comprised of the Peierls stress, τ_p , and strength from dislocation interactions, $\hat{\tau}(\rho)$. Note that $\hat{\tau}(\rho)$ appears in both the athermal and thermal terms of Eq 2. The parameters ϕ_A and ϕ_T provide a means to apportion the forest dislocation contribution between the thermal and athermal terms.

Contributions from Molecular Statics and Dynamics

The Peierls stress appearing in Eq. 2 and later relations was calculated through molecular statics simulations at 0K [1]. The pressure dependence of τ_p for screw dislocations was determined to scale with shear modulus over a wide range of pressures. In order to include this pressure dependence but not have the strength model tied to a specific shear modulus parameterization, the pressure scaling is applied through an independent parameter.

$$\tau_p = \tau_{p0}(1 + \zeta P) \tag{3}$$

The pressure scaling parameter will be set equal to the pressure dependence of the shear modulus for the current parameterization, but providing an independent parameter allows the flexibility to choose other values.

Molecular dynamics simulations were used to determine the relationship between dislocation velocity and shear stress. The tantalum MGTP potential was used to simulate motion of a single screw dislocation at a range of temperatures and applied shear strain rates. An average dislocation velocity and shear stress on the simulation box were determined for each calculation, and the results are shown as data points in Figure 1.

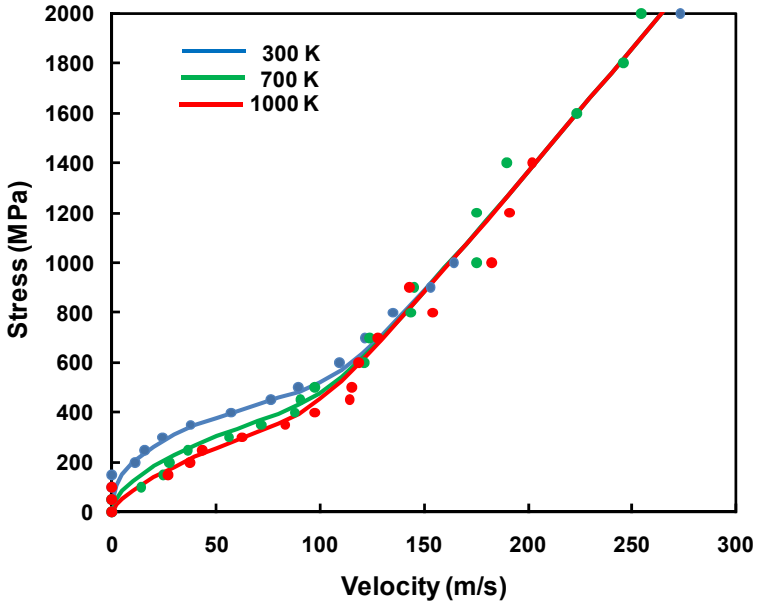

Figure 1. Shear stress as a function of screw dislocation velocity at several temperatures.

The numerical data clearly show two regimes. At lower dislocation velocities and stresses the dislocation motion thermally activated. The temperature sensitivity is evident at these lower velocities. At higher velocities and stresses the numerical data suggest a linear mobility relationship with little temperature sensitivity. It is assumed to be independent of temperature for the model fits. The transition between the two regimes occurs over a relatively small strength range near the Peierls stress.

Curve fits were constructed for each regime independently, and the resulting functions were connected with a smooth transition function. The fits are plotted as solid lines in Figure 1. The functions are normalized by the Peierls stress, τ_p , giving the nondimensional relations

$$\tilde{\tau}_{\mathrm{Therm}} = \alpha_0 \exp\left(\frac{\mathrm{T}}{\alpha_t}\right)\left\{\exp\left[\left(\beta_0 + \frac{\mathrm{T}}{\beta_t}\right)\ln\left(\frac{v}{c_0} + \widetilde{v_0}\right)\right] - \exp\left[\left(\beta_0 + \frac{\mathrm{T}}{\beta_t}\right)\ln(\widetilde{v_0})\right]\right\} \qquad (4)$$

in the thermally activated regime and

$$\tilde{\tau}_{\mathrm{Drag}} = \langle\ \chi_0\left[\frac{v}{c_0} - \chi_1\right] \Big/ \sqrt{1 - \left({}^{v}/_{c_0}\right)^2}\ \rangle \qquad (5)$$

in the drag regime. The angled brackets in Eq. 5 imply that the drag strength should be zero if the function evaluates to a negative value. The denominator in Eq. 5 is intended to elevate the stress as the dislocation velocity approaches the shear wave speed. Both Eqs 4 and 5 give zero stress at zero dislocation velocity to provide a continuous function as the strain rate approaches zero.

Equations 4 and 5 are joined with the transition function

$$\tau^* = \sqrt[5]{\tilde{\tau}_{\mathrm{Therm}}^5 + \tilde{\tau}_{\mathrm{Drag}}^5} \qquad (6)$$

τ^* is the dimensionless multiplier in Eq. 2. Multiplying by the Peierls stress within Eq. 2 provides pressure dependence and imparts the correct dimensionality. The exponent 5 was determined to provide a good fit to the molecular dynamics data at the transition. Other than the temperature, T, and the reference sound speed, c_0, the remaining parameters in Eqs. 4-6 are fitting parameters given in Table 1.

Contributions from Dislocation Dynamics

The dislocation mobility relations in Eqs 4-6 were implemented in the dislocation dynamics code to simulate the evolution of dislocation density and strain hardening. The dislocation density saturates at approximately 10% strain in calculations that were run sufficiently long. Saturation densities were also estimated from simulations to lower strains and from strain rate jump tests. These were used to determine a functional dependence for the saturated dislocation density. The saturation density was found to depend strongly on strain rate and weakly on temperature. Figure 2 shows the strain rate dependence along with a power law equation fit,

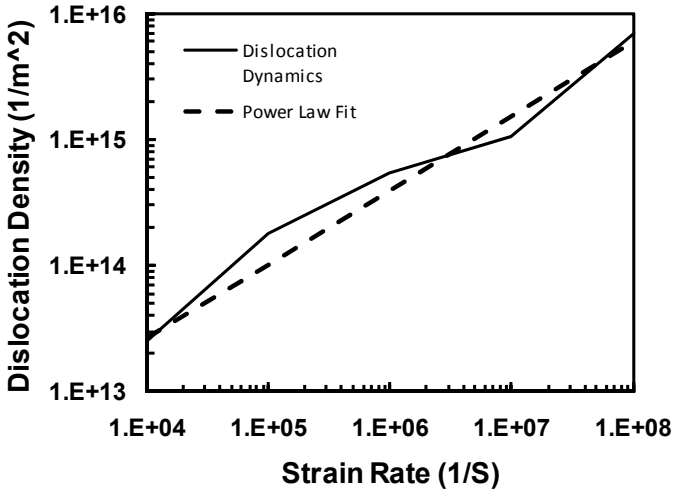

Figure 2. Saturation dislocation density as a function of strain rate.

Table 1 Model Parameters

b_0	$2.86\text{x}10^{-10}$		ϕ_A	1.0
τ_a	15 MPa		ϕ_T	0.0
τ_{p0}	525 MPa		η	1.0
ζ	$1.45\text{x}10^{-5}$ MPa^{-1}		ρ_{0s}	$1.1266\text{x}10^{11}$ m^{-2}
c_0	2000 m/s		$\dot{\varepsilon}_N$	1 s^{-1}
$\tilde{v}_0$	10^{-9}		S_o	650
α_0	2.3643		n	0.59
α_t	1127 K		R	$1\text{x}10^{17}$ m^{-2}
β_0	0.2757		β	0.4
β_t	2548 K		G_0	69000 MPa
χ_0	37.166		M	3.08
χ_1	0.03075			

$$\rho_{\text{Sat}} = \rho_{0S}\left(\frac{\dot{\varepsilon}^p}{\dot{\varepsilon}_N} + S_0\right)^n \tag{7}$$

Since errors in extrapolating to the saturation density appear to be as large as temperature dependence, the saturation density is taken to be independent of temperature.

Dislocation density is assumed to increase proportionally to existing density as there are more obstacles to react and create additional loops. The dislocation density decreases by annihilation within a capture radius which is assumed to depend quadratically on density. In primitive form, the evolution equation is written as a function of dislocation density and velocity

$$\dot{\rho} = (H\rho - A\rho^2)v \tag{8}$$

However, in light of Orowan's relation, Eq. 1, it is possible to rewrite the evolution relation in terms of plastic strain rate and saturation density.

$$\dot{\rho} = R\left(1 - \frac{\rho}{\rho_{\text{Sat}}}\right)\dot{\varepsilon}^p \tag{9}$$

where R is the growth rate for dislocation density far from the saturation density. Closed form integration of Eq. 9 over a time step provides the dislocation density at the end of an arbitrarily sized time increment in terms of the value at the beginning of the time step, ρ_t, and the saturation value.

$$\rho = \rho_t \exp\left(-R\frac{\dot{\varepsilon}^p \Delta t}{\rho_{Sat}}\right) + \rho_{\text{Sat}}\left[1 - \exp\left(-R\frac{\dot{\varepsilon}^p \Delta t}{\rho_{\text{Sat}}}\right)\right] \tag{10}$$

What remains is specification of how the evolving dislocation density contributes to strain hardening through $\hat{\tau}(\rho)$ in Eq. 2. Experimental evidence collected over many years suggests that the strength increases proportionally to the square root of the dislocation density. The proportionality constant is commonly assumed to be the product of the Burger's vector, the shear modulus and an order one constant. That common form is adopted here, as illustrated by Eq. 11.

$$\tau(\rho) = \beta b G_0(1 + \zeta P)\sqrt{\rho} \tag{11}$$

In Eq. 11, the pressure dependence of the shear modulus is represented explicitly as it is for the Peierls stress in Eq. 3. This uncouples the strength model from the shear modulus model. The Burger's vector, on the other hand, is the current value computed from the reference value, b_0, and the current volume strain.

Comparison with data

The model presented above was constructed entirely from multiscale simulation predictions with no adjustments to match experimental data. In order to determine how well the model represents observation, comparisons are made with several data sets available in the literature.

Figure 3 shows the temperature dependence of strength measured under a broad range of experimental conditions. Many of the data sets are at strain rates of 10^{-4} sec^{-1} and $3x10^{3}$ sec^{-1}. Predictions from the multiscale model were calculated at these two rates assuming a saturated dislocation density from Eq. 7. These are plotted as solid and dashed lines along with the data in Figure 3. The model predicts the strength level fairly well, but the temperature dependence of the strength predictions is not as great as it is in the experiments.

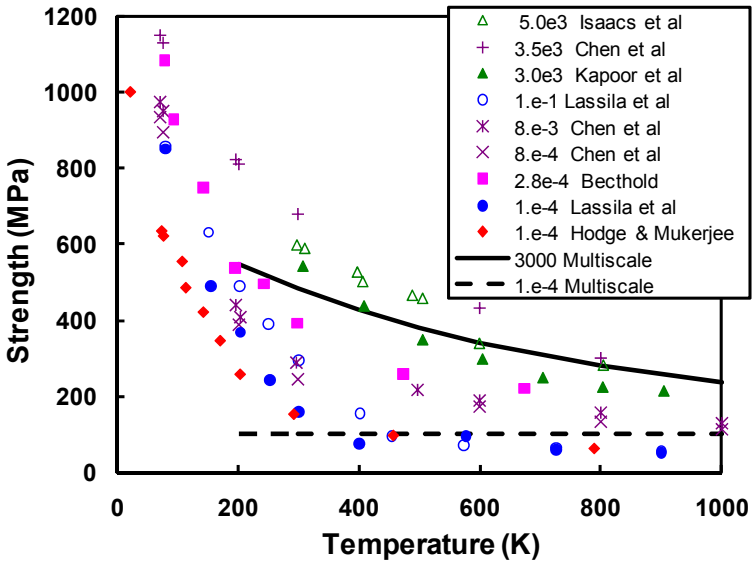

Figure 3. Comparison of the temperature dependence of the multiscale model predictions with a range of data at several strain rates.

The molecular dynamics data used to construct the model were provided at 300K, 700K and 1000K. Results extrapolated outside of this range, particularly below 300K, tend to have the largest deviations. The MD simulations should be repeated at lower temperatures to determine whether or not the experimentally observed temperature sensitivity is replicated

A similar comparison is made by plotting the strength predictions against strain rate at 300K in Figure 4. The agreement between the data and predictions is not favorable at lower rates, and it is observed that the strain rate sensitivity predicted by the model is significantly greater than in the experiments. As with the temperature sensitivity, part of the reason for the poor fit may be the stain rate range over which velocity data were calculated in the MD simulations. Only velocities corresponding to strain rates of 10^{4} sec^{-1} and higher were available to fit the continuum model.

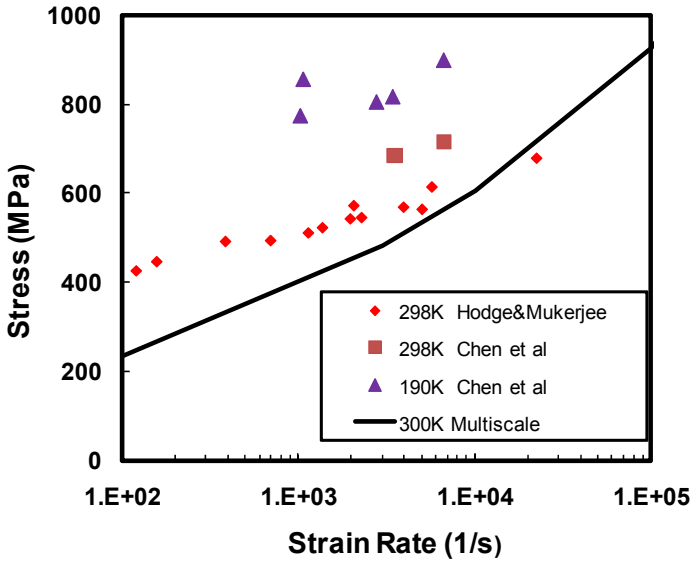

Figure 4. Comparison of the strain rate dependence of the multiscale model predictions with data from several studies.

The model was implemented as part of the MS material model library in ALE3D for use in full-scale hydrodynamic calculations. An example illustrating the model predictions in the dynamic range is the simulation of a tantalum gas gun experiment with a multi-component flyer comprised of PMMA (6.16mm), tungsten (1.6 mm) and sapphire (3.171 mm) disks impacting a tantalum target (5.0225 mm) backed by a sapphire window [3]. The configuration is shown in Figure 5. The impact velocity was approximately 133 m/s.

Velocimetry at the tantalum-window interface is shown as the short-dashed line in Figure 6a (taken from [3]) along with results from two models (solid and long dashed lines) fit to the data in the original paper. Figure 6b shows one of the same model fits as the gray line along with the multiscale model prediction as the dark line. The multiscale model predicts a low HEL compared to the experiment, but the flattened hump from the multiscale model at 0.0065 m/s is in better agreement with the experiment than the original model fit. Another prominent feature is the softened pullback at approximately 2 μs. In the original paper a Baushinger effect was used to capture a gradual pullback. The multiscale model produces a similar effect through evolution of internal history variable.

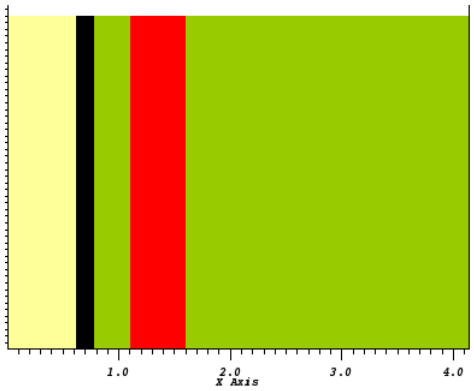

Figure 5. Material layout for gas gun experiment

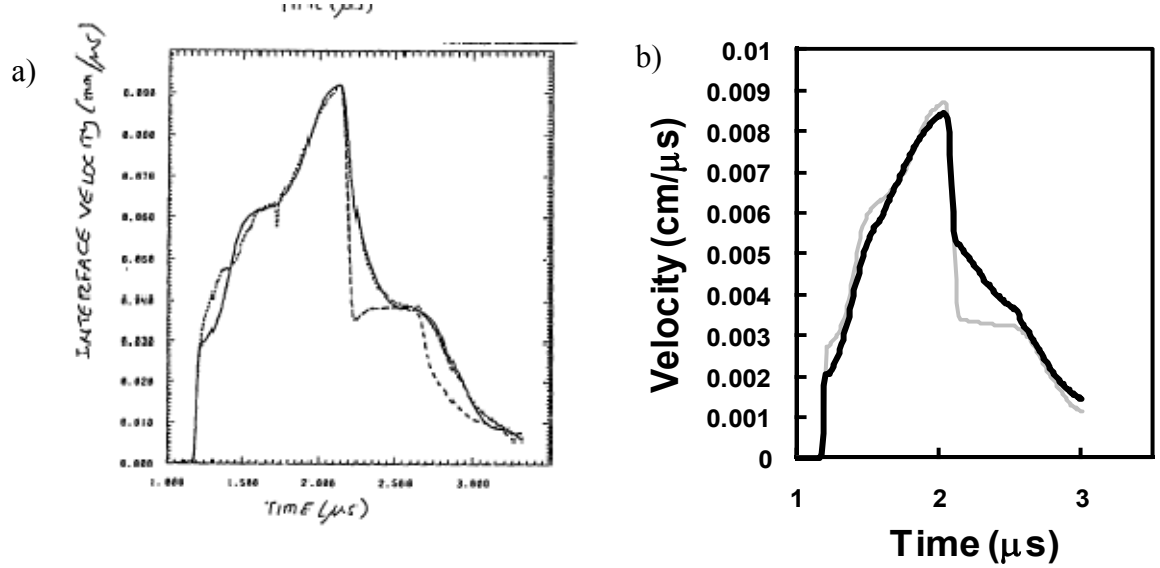

Figure 6. Results from a) gas gun experiment and original two models [3] and b) the multiscale tantalum model.

High Rate Application

One of the target applications for the multiscale tantalum model is simulation of laser driven Rayleigh-Taylor instability experiments. Here high-pressure plasma impinges on a surface with prescribed sinusoidal perturbations. Plastic deformation of the surface is unstable under the high pressure loading and the perturbations grow.

To evaluate the model robustness and behavior for these applications, a pressure boundary condition was imposed on the surface of a 49 μm thick tantalum target glued with a 5 μm thick layer of epoxy to a 500 μm thick Lithium-Floride window [4]. The initial ripple amplitude was 3 μm and the wavelength was 50 μm. A blow-up of the initial target surface is shown in Figure 7a and the pressure drive is depicted in Figure 7b.

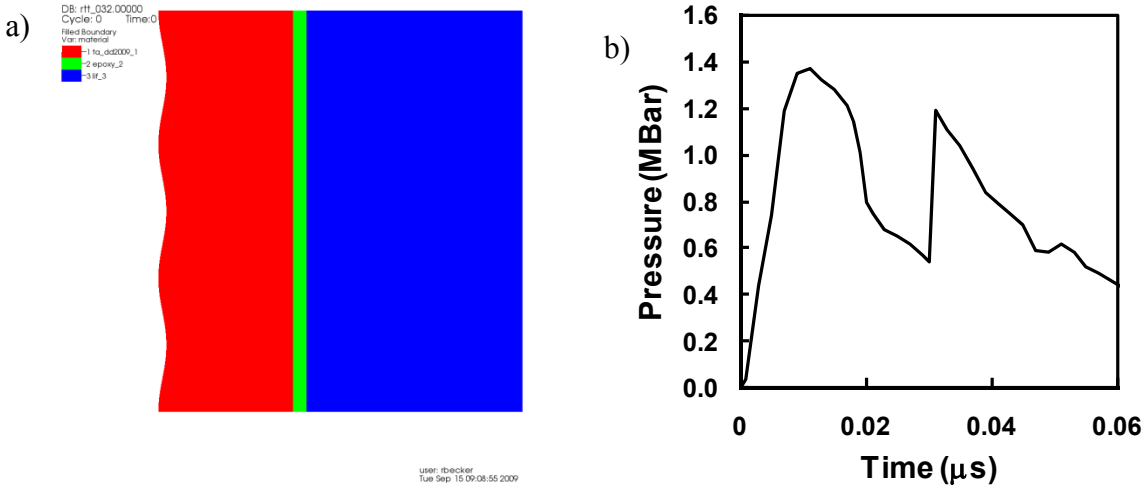

Figure 7. Set-up for Rayleigh-Taylor growth simulations: a) initial rippled target surface and b) pressure drive

Plots of dislocation velocity indicate that the ripple growth early in the simulation is in the phonon drag regime while growth at later times may drop below the drag threshold. The ripple growth in the experiments is determined by quantitative radiography which looks at the target thickness in addition to any transient density variations. For these simulations the growth factor is characterized by the current peak to valley distance normalized by the original amplitude. The drive is relatively weak compared to the material strength, and the ripple growth is small. A plot of the growth factor evolution is shown in Figure 8 along with predicted growth factors for the Steinberg-Guinan, Steinberg-Lund and Preston-Tonks-Wallace models. The results suggest that the multiscale model is stiffer that these. However, the stress in the Steinberg-Lund model hits the prescribed cap, and that model would be much stronger if the cap were raised.

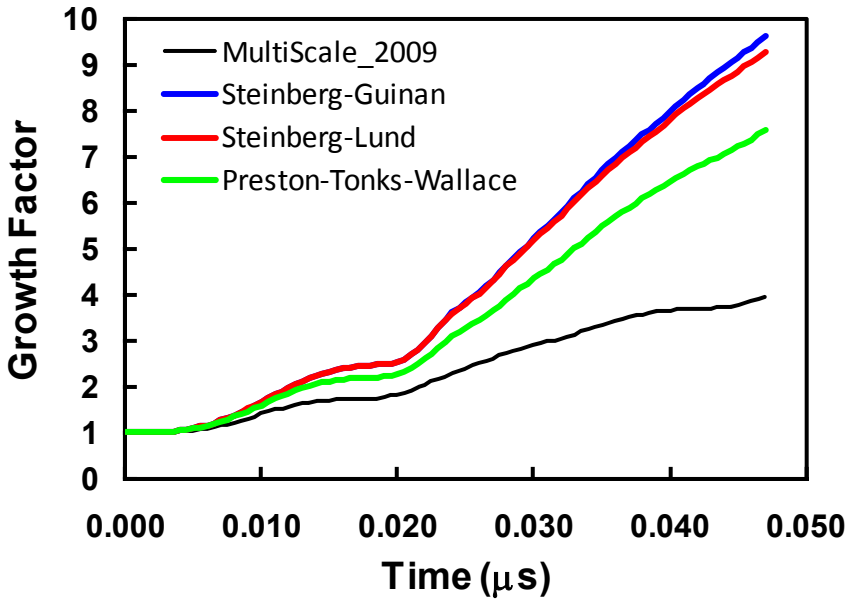

Figure 8. Predicted Rayleigh-Taylor growth factors

Discussion

A second generation multiscale model for tantalum was developed from molecular dynamics and dislocation dynamics simulation data. The underlying multiscale calculations were run at relatively high strain rates so the model fits are most appropriate for strain rates above 10^3 sec^{-1}. Direct measurement of material strength is difficult to impossible in this range, so the model cannot be validated directly over much of the range in which it was constructed. However, comparisons at 10^3 sec^{-1} show reasonable agreement, and it is anticipated that the model predictions would also be reasonable at higher rates. Significant data exist at lower strain rates, and the agreement between model and data degrades as the strain rate is reduced. Whether this is an issue with model extrapolation or with the underlying simulation data has not been determined at this time.

The situation is similar with temperature. The model was constructed using simulation data at 300K, 700K and 100K, and the comparisons with data at10^3 sec^{-1} seem reasonable in that temperature range. The strength predictions extrapolated to lower temperatures are not in good

agreement with the available data, and one is not sure whether the problem is with extrapolation or deficiencies in the underlying data that aren't apparent in the narrower temperature range.

In the course of running the multiscale simulations, several unexpected trends appeared that have prompted a closer look at the underlying physics, parameterization of the lower scale models, and how the codes are run. One series of simulations involved running the molecular dynamics code at elevated pressure to determine the pressure dependence of the dislocation mobility relations. The pressure dependence was not following the anticipated trends, so further research and validation are required before accepting the results. Another question arose when comparing the temperature sensitivity of the dislocation dynamics predictions to existing data. The results showed considerably less temperature sensitivity than the input mobility relations. The reason for this is not understood and is also being investigated.

The unexpected results compelled a change in plan for constructiing the current continuum model. Rather than basing the model on multiscale simulation results that are not understood or are questionable, those results were disregarded for purposes of model construction. A safe and conservative approach was taken for including the pressure and strain rate dependence. Consequently, the model follows expected trends, reflecting the traditional assumptions. However, this conservative approach disregards one of the main drivers for the multiscale modeling effort – determining strength dependencies at extreme conditions where definitive experiments are not possible. Therefore, the issues encountered must be resolved. Understanding and trusting results from all lengths scales is crucial in the multiscale modeling paradigm. The uncertainties uncovered here have prompted a renewed look at the quantitative predictions of models at all length scales.

Acknowledgements

Support of the ASC-PEM program is gratefully acknowledged. This work performed under the auspices of the U.S. Department of Energy by Lawrence Livermore National Laboratory under Contract DE-AC52-07NA27344. LLNL-TR-417075

References

[1] Arsenlis, A., "L2 Multiscale Strength Milestone Review," *Presentation to the L2 Milestone committee*, 2007

[2] Becker, R, Arsenlis, A., Marian, J., Rhee, M., Tang, M. and Yang, L "Continuum level formulation and implementation of a multi-scale model for vanadium," Aug., 2009, LLNL-TR-416095.

[3] Steinberg, D.J., "Modeling release behavior in shocked tantalum," *1995 APS Topical Conference on Shock Compression of Condensed Matter*, Seattle, WA, August 13-18, 1995, UCRL-JC-121814.

[4] Park, H-S., Private communication.